Contents lists available at ScienceDirect

Nuclear Instruments and Methods in Physics Research A

journal homepage: www.elsevier.com/locate/nima

Radiation damage in n-type silicon diodes after electron irradiation with energies between 1.5 MeV and 15 MeV

Roxana Radu [a,b,*], Eckhart Fretwurst [a], Robert Klanner [a], Gunnar Lindstroem [a], Ioana Pintilie [b]

[a] Institute for Experimental Physics, Hamburg University, Hamburg, Germany
[b] National Institute of Materials Physics NIMP, Bucharest, Romania

ARTICLE INFO

ABSTRACT

Radiation damage in silicon, caused by the creation of point and cluster defects due to energetic charged hadrons and neutrons, results in a serious degradation of silicon-sensor performance and limits their lifetime. So far not all the defects are understood. The work presented here focuses on the study of radiation damage by electrons of different kinetic energies, from 1.5 MeV to 15 MeV, in order to study the differences between point- and cluster-related defects. The introduction rate of vacancy-related point defects and of so-called clustered regions was investigated as a function of electron energy. It is shown that the ratio between cluster dominated and point defect formation increases with increasing electron energy. 1.5 MeV electrons create only point defects, and the formation of cluster defects starts already at 3.5 MeV. To study the defect kinetics, isothermal annealing at 80 °C and isochronal annealing measurements were performed.

© 2013 Elsevier B.V. All rights reserved.

1. Introduction

A detailed study regarding the feasibility of the LHC (Large Hadron Collider) luminosity and energy upgrade has been done in 2002 at CERN [1]. The upgrade to a 10 times increased luminosity up to 10^{35} cm^{-2} s^{-1}, foreseen for 2020, will require silicon tracking detectors with substantially improved radiation tolerance, especially for the innermost regions of the LHC detectors where they will be exposed to very high fluences of charged and neutral particles.

The main mechanisms responsible for radiation damage are bulk and surface damage leading to microscopic defects in the bulk (crystal), and damage effects in the surface-passivation layer and the Si–SiO$_2$ interface due to ionizing radiation, respectively [2]. The presented work is focusing on the radiation damage due to Non-Ionizing Energy Loss (NIEL) resulting in displacement damage in the silicon bulk. The main macroscopic properties affected by radiation-induced defects are: (i) change in the effective doping concentration with consequences for the voltage needed to achieve total depletion of the silicon sensor, (ii) fluence-proportional increase in the leakage current caused by the creation of generation centers, and (iii) deterioration of the

charge-collection efficiency due to charge-carrier trapping causing a reduction of the signal produced by minimum ionizing particles (mips) in the sensor. The microscopic origin of these effects is not completely understood. In recent years various systematic studies have been carried out to identify the main defects responsible for radiation damage of silicon particle detectors as well as their formation kinetics [3]. In order to further develop ultra-radiation-hard silicon sensors, it is of importance to gain more insight into the generation and kinetics of electrically active defects (point and cluster like centers), which are responsible for the changes in the macroscopic properties. Instead of comparing the damage by high-energy protons (mixture of point and cluster effects) with the damage by MeV neutrons (predominantly cluster effects) followed so far by the CERN-RD50 Collaboration [3–12], the approach in this work is to scan the defect formation from point defects to clusters by irradiating the silicon sensors with mono-energetic electrons in the energy range from 1.5 to 15 MeV. Specifically, the irradiations were performed with electrons with kinetic energies of 1.5 MeV, 3.5 MeV, 6 MeV and 15 MeV.

2. Materials and techniques

Several types of n-type silicon crystals have been investigated: Standard and Diffusion Oxygenated Float Zone (STFZ and DOFZ) and Epitaxial Silicon grown on highly doped Czochralski substrate (EPI-ST) materials. The material parameters are displayed

* Corresponding author at: Institute for Experimental Physics, Hamburg University, Hamburg, Germany. Tel.: +40 21 369 0185x130.
E-mail addresses: roxana.radu@desy.de, roxana@infim.ro (R. Radu).

Table 1
Material parameters for the pad diodes investigated: d is the crystal thickness, N_D the n-doping concentration, $<[O]>$ the average oxygen concentration from SIMS measurements, and ρ the resistivity.

Material	Orientation	d [μm]	N_D [cm^{-3}]	$<[O]>$ [cm^{-3}]	ρ [Ωcm]	O$_2$ diffusion
EPI	$<111>$	50	6×10^{13}	1×10^{17}	50	–
STFZ	$<100>$	280	8×10^{11}	1×10^{16}	5×10^3	–
DOFZ	$<100>$	280	8×10^{11}	1.2×10^{17}	5×10^3	72 h/1150 °C

in Table 1. From the measured depth profiles of the oxygen concentration using Secondary Ion Mass Spectroscopy (SIMS) the average values are given in Table 1. It should be mentioned that the large average oxygen concentration in EPI-ST material is due to the in-diffusion of oxygen from the Czochralski substrate during epitaxial growth. On these materials p$^+$–n–n$^+$ pad diodes were fabricated by the company CiS (Forschungsinstitut für Mikrosensorik und Photovoltaik GmbH) [13]. The p$^+$ implant has an area of 25 mm^2 surrounded by a p$^+$ ring. The n$^+$ electrode covers the total 1 cm^2 area of the rear side. Laser-light injection was made possible via a small opening in the aluminum contact at the front side, and an aluminum grid as rear electrode.

As stated in Section 1, irradiations with four electron energies have been performed in order to study the transition from the creation of only point defects at low energies, to predominantly cluster defects at higher energies. The irradiation with 1.5 MeV electrons was performed at the facility of the Energy and Nuclear Research Institute (IPEN-CNEN/SP), Sao Paolo, Brazil [14], the 3.5 MeV electron irradiation at the Belarusian State University, Minsk, Belarus [15], the 6 MeV irradiation at the Metrology Institute PTB, Braunschweig, Germany [16], and the 15 MeV irradiation at the ELBE facility at the Helmholtz-Zentrum Dresden-Rossendorf, Germany [17].

For all diodes the macroscopic properties before and after irradiation were obtained by means of Current–Voltage (IV) and Capacitance–Voltage (CV) measurements. From the CV curves the voltage at full depletion (V_{dep}) and the saturation capacitance (C_{end}) were determined, allowing the calculation of the effective doping concentration (N_{eff}) and the sensitive thickness of the sensor. From the IV curves, the dark current at full depletion (I_{leak}) was extracted.

The main part of the present work deals with the measurement and analysis of radiation-induced electrically-active defects. For this purpose the most sensitive methods used are the Capacitance Deep Level Transient Spectroscopy (DLTS) [18] and the Thermally Stimulated Current (TSC) technique [19]. From the spectra measured with these methods the following defect parameters can be determined: activation energy (E_a), capture cross-sections (σ_n and σ_p) and defect concentration (N_T). In our DLTS system a Fast Fourier Transformation is applied to the measured transient for evaluation of the emission-time constant and trap concentration [20,21]. The DLTS technique can only be applied for defect concentrations which are 10 times smaller compared to the initial doping concentration N_D, thus for an irradiation fluence $\leq 10^{12}$ e/cm^2. On the other hand, the TSC method can be used for studies at much higher fluences up to 10^{15} e/cm^2. A detailed description of the TSC procedure and analysis of the recorded spectra when the method is applied on diodes with a high density of defects can be found in [4,9,22]. Thus, for a correct evaluation of the defects concentration, activation energy and capture electrons/holes cross-sections the TSC experiment has to be performed on fully depleted diodes having the guard ring grounded. The mathematical formalism used in deconvoluting the TSC spectra and determination of the entire density of defects is explained in detail

in Refs. [4,9]. Once the defect concentrations are determined from the DLTS and/or TSC spectra, the introduction rates of the detected defects can be calculated by dividing the concentration by the irradiation fluence.

3. NIEL scaling violation

Many experiments have shown that bulk-damage parameters scale independently of particle type and energy with fluence if normalized to the Non Ionizing Energy Loss (NIEL). Numerous results obtained by the CERN-RD48 and CERN-RD50 collaborations [3,23] have shown that not all damage parameters follow NIEL scaling [24]. However, for the current related damage parameter $\alpha = \Delta I/(V\Phi)$ (ΔI is the radiation-induced change of the dark current, V the depleted volume, and Φ the fluence) the scaling with NIEL was shown to be valid for radiation damage induced by neutrons and charged hadrons. One question is, whether the NIEL scaling of α is also valid for electrons in the energy range between 1.5 MeV and 15 MeV. Fig. 1 shows a comparison of the α values measured in this work with the calculated NIEL values for electrons presented in [25,26]. The dots represent the experimental α values, the triangles the "classical" NIEL values from [25], and the squares the "effective" NIEL values from [26]. A significant difference between the energy dependence of α and the "classical" NIEL is observed, while the "effective" NIEL describes the energy dependence of α much better at least at low electron energies, up to 6 MeV. One has to keep in mind that the "classical" NIEL predicts only the total number of atomic displacements, i.e. the number of Frenkel pairs (vacancy V–interstitial I pairs) when a particle traverses the material [27]. It does not take into account V–I recombination processes or the final formation of stable defects. The "effective" NIEL calculation however is based on molecular-dynamic simulations [26,28] which take into consideration the development of the initial energy transferred to the lattice atoms into the final formation of stable displacements (defects). As can be seen from Fig. 1, the "effective" NIEL values are smaller than the "classical" NIEL values by up to one order of magnitude at energies of about 1 MeV.

4. TSC results as function of electron energy

Using the TSC method we were able to measure spectra in a wide range of electron fluences (10^{13}–10^{15} cm^{-2}) for all energies under study. Fig. 2a) shows a comparison of TSC spectra for the
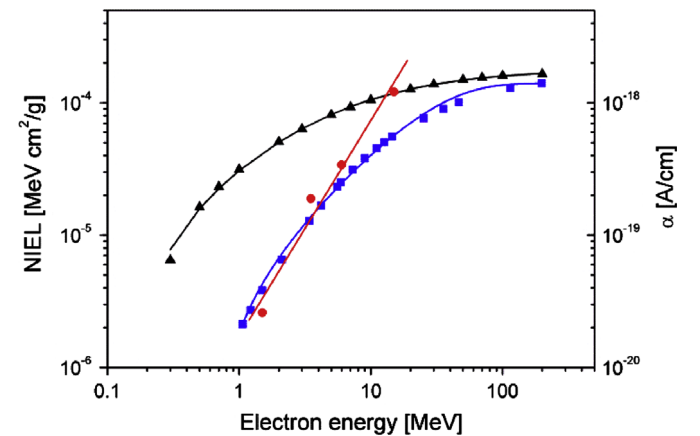

Fig. 1. Comparisons of the current-related damage for electrons α (dots) with the "classical" (triangles) and "effective" (squares) NIEL values as function of electron energy for EPI-ST (electron kinetic energy: 1.5 MeV) and DOFZ (3.5, 6, and 15 MeV) directly measured after irradiation.
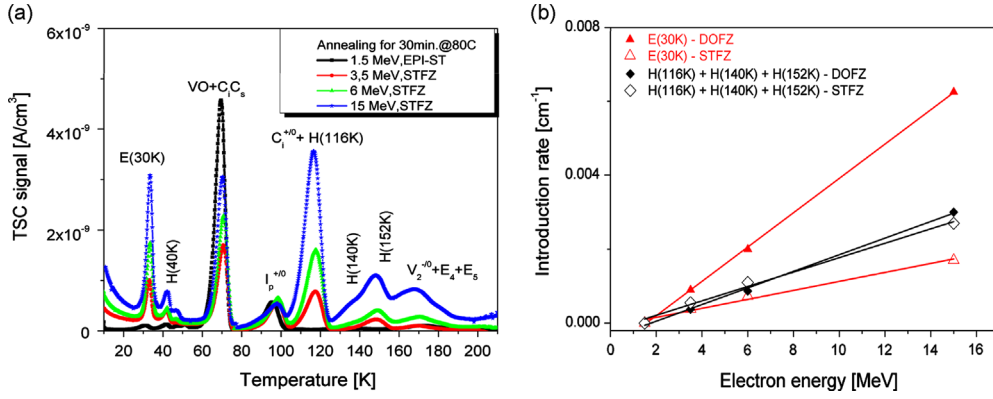
Fig. 2. (a) TSC spectra for different electron energies measured on EPI-ST (1.5 MeV) and STFZ materials (3.5, 6, and 15 MeV) after annealing for 30 min at 80 °C, scaled to a fluence of $\Phi = 6 \times 10^{14}$ cm^{-2}, and (b) introduction rate for E (30 K) and H defects versus electron kinetic energy, after annealing for 30 min at 80 °C in STFZ and DOFZ materials.

four electron energies used to irradiate, EPI-ST and STFZ diodes. The obtained TSC spectra were recorded during the heating up with a constant heating rate $\beta = 0.183$ K/s and with a high enough applied reverse bias to ensure the full depletion of the diode over the whole TSC temperature range (100 V for EPI-ST and 300 V for STFZ). The trap filling was performed at 10 K with a 2 mA forward current. The electrically active defects detected in this work, their trapping parameters (activation energy and capture cross-sections) and presumable structure assignment are given in Table 2. Given the different thicknesses of the investigated diodes (50 μm for EPI-ST diode and 280 μm for the STFZ diodes), as well as the differences in the irradiation fluence, a direct comparison of the TSC spectra measured on different samples can be done if the TSC signal is normalized to the active volume and scaled to the same fluence ($\Phi = 6 \times 10^{14}$ cm^{-2} in Fig. 2a). A comparison between EPI-ST and DOFZ (not shown here) was done and the results agree with the statements below. It can be seen that for 1.5 MeV only point defects (VO+C_iC_s, $I_p^{(+/0)}$ and V_2) are created. A much larger concentration of single vacancy related defect VO in the EPI-ST is of course also due to the higher oxygen concentration (Table 1). With increasing electron energy the recoil energy of the displaced atoms also increases, leading to the creation of disordered regions with a high density of vacancies and interstitials, also known as cluster defects. Previous irradiation experiments have revealed the existence of a group of cluster-related defects, H (116 K), H (140 K) and H (152 K), traps for holes with acceptor-type levels in the lower half of the band gap, and a shallow defect E (30 K), a trap for electrons with a donor level in the upper half of the band gap, with direct impact on the device characteristics [10,11]. These defects are not observed for ^{60}Co-gamma irradiation, an indication that they are extended defects [11,30–32]. These are expected to form for electrons energies larger than 8 MeV [29]. However, the present work brings evidence that the cluster related defects (H (116 K), H(140 K) and H(152 K)) are forming already for electrons of 3.5 MeV energy. It was found that the introduction rate of cluster-related deep hole traps and of the shallow donor increase with increasing electron energy (Fig. 2b). It should be mentioned that the TSC peak centered at 170 K increases also with increasing energy. This peak can be attributed to the higher-order vacancy defects (V_2, $E_4 = V_3^{=/-}$, $E_5 = V_3^{-/0}$) and a deep hole trap which could not be identified so far. In Fig. 2b) the energy dependence of the introduction rates for the E (30 K) defect and the sum of H (116 K), H (140 K) and H (152 K) defects is shown for the STFZ and DOFZ materials. For the sum of H (116 K), H (140 K) and H (152 K) defects the introduction rates for the two materials are identical, which means that there is no oxygen dependence for these defects. However, for E (30 K) the introduction rate is almost 3 times larger

in DOFZ material. It is concluded that the generation of E (30 K) is oxygen dependent, which means that it is not an intrinsic defect. By now no conclusive measurements exist to identify the chemical structure of these defects.

Annealing experiments were carried out at constant temperature (isothermal at 80 °C), and isochronal at elevated temperatures up to 300 °C, in order to investigate the kinetics of these defects. It can be noticed, from Fig. 3, that the concentrations of the H (116 K), H (140 K) and H (152 K) defects first increase with annealing temperature, reach maxima at around 180 °C, and then start to anneal out. For E (30 K) the concentration reaches a maximum at around 220 °C and drops rapidly at higher temperatures. These defects were found to have an impact on the time and temperature evolution of the effective doping, N_{eff}, in n-type diodes [10,11]. The defect studies by TSC were used to predict the annealing effects of N_{eff} and to compare the results with values determined from C–V measurements. The evolution of the defect concentrations with time after irradiation (not shown here) does not fully describe the annealing of N_{eff} as determined from C–V measurements after electron irradiation. An effort to relate the macroscopic properties to microscopic defects in electron-irradiated samples is under way.

5. Material dependence

A comparison of the TSC spectra obtained for STFZ and DOFZ diodes after irradiation with the same electron energy of 6 MeV and same fluence of 10^{15} cm^{-2} is displayed in Fig. 4a). It should be noted that for STFZ, due to the very low oxygen concentration, an overlap of H (116 K) and $C_i^{+/0}$ can be seen directly after irradiation. Therefore the TSC spectra are shown after annealing for 60 minutes at 80 °C, when the carbon interstitials have totally vanished due to the transformation into C_iC_s and C_iO_i, and the full concentration of H (116 K) can be measured. One can clearly see that, while the overall H-defect concentrations (H (116 K), H (140 K) and H (152 K)) are about the same for the two materials, the E (30 K) concentration is much larger in DOFZ. The difference between the two materials is also given by the appearance of the I_p defect in STFZ. This defect is a point defect, measured after 1.5 MeV electron irradiation as stated in Section 4. In previous studies [30–32] with γ irradiation the I_p defect was found to be responsible for the type inversion in oxygen-lean material. It was detected so far in three charge states (−, 0, and +), with two levels in the band gap: a donor level in the lower part (E_V+0.23 eV), and an acceptor level at the middle of the gap (E_C−0.55 eV).

Table 2

Labeling of radiation induced electron and hole traps detected in this work. Defect parameters, $\sigma_{n,p}$, the capture cross-section holes/electrons, and E_a, the activation energy, have been determined from TSC or DLTS measurements. The assignment to a certain defect structure is based on the values of trapping parameters and annealing behavior reported earlier in the literature for several defect structures. The LC and N_{eff} stand for the leakage current and the effective doping concentration, respectively.

| Defects	$\sigma_{n,p}$ [cm^2]	E_A [eV]	Assignment/references	Impact on the diodes electrical characteristics at room temperature
E(30 K)	$\sigma_n = 2.3 \times 10^{-14}$	$E_C-0.1$	Electron trap with a donor level in the upper half of the Si bandgap [11]	On the N_{eff} by introducing positive space charge
H(40 K)	$\sigma_p = 1.7 \times 10^{-15}$	$E_V+0.09$	Hole trap [11]	
VO$_i^{-/0}$	$\sigma_n = 1.44 \times 10^{-14}$	$E_C-0.176$	VO$_i^{-/0}$ [40]	
C$_i$C$_s^{-/0}$	$\sigma_n = 1.4 \times 10^{-14}$	$E_C-0.171$	C$_i$C$_s^{A-/0}$ [41,42]	
I$_p^{+/0}$	$\sigma_p = (0.5-9) \times 10^{-15}$	$E_V+0.23$	Donor level of V$_2$O or of a still unkown C related defect [11,30]	
I$_p^{0/-}$	$\sigma_n = 1.7 \times 10^{-15}$ $\sigma_p = 9 \times 10^{-14}$	$E_C-0.55$	Acceptor level of V$_2$O or of a still unkown C related defect [11,30]	On the N_{eff} by introducing negative space charge and on LC
C$_i^{+/0}$	$\sigma_n = 1.11 \times 10^{-15}$ $\sigma_p = 4.28 \times 10^{-15}$	$E_V+0.284$	C$_i^{+/0}$ [21]	
V$_2^{-/0}$	$\sigma_n = 2.1 \times 10^{-15}$	$E_C-0.424$	V$_2^{-/0}$ [21]	
E$_4$	$\sigma_n = 1 \times 10^{-15}$	$E_C-0.38$	V$_3^{=/-}$ [38]	On LC
E$_5$	$\sigma_n = 7.8 \times 10^{-15}$	$E_C-0.46$	V$_3^{-/0}$ [38]	On LC
H(116 K)	$\sigma_p = 4 \times 10^{-14}$	$E_V+0.33$	Hole trap with an acceptor level in the lower part of the Si bandgap—Extended defect (cluster of vacancies and/or interstitials) [10,11]	On the N_{eff} by introducing negative space charge
H(140 K)	$\sigma_p = 2.5 \times 10^{-15}$	$E_V+0.36$	Hole trap with an acceptor level in the lower part of the Si bandgap—Extended defect (cluster of vacancies and/or interstitial) [10,11]	On the N_{eff} by introducing negative space charge
H(152 K)	$\sigma_p = 2.3 \times 10^{-14}$	$E_V+0.42$	Hole trap with an acceptor level in the lower part of the Si bandgap—Extended defect (cluster of vacancies and/or interstitial) [10,11]	On the N_{eff} by introducing negative space charge
H(87 K)	$\sigma_p = 0.3 \times 10^{-15}$	$E_V+0.193$	V$_3^{0/+}$ [37]	
H(98 K)	$\sigma_p = 1.2 \times 10^{-15}$	$E_V+0.234$	V$_2$O$^{0/+}$ V$_3$O$^{0/+}$ [37]	
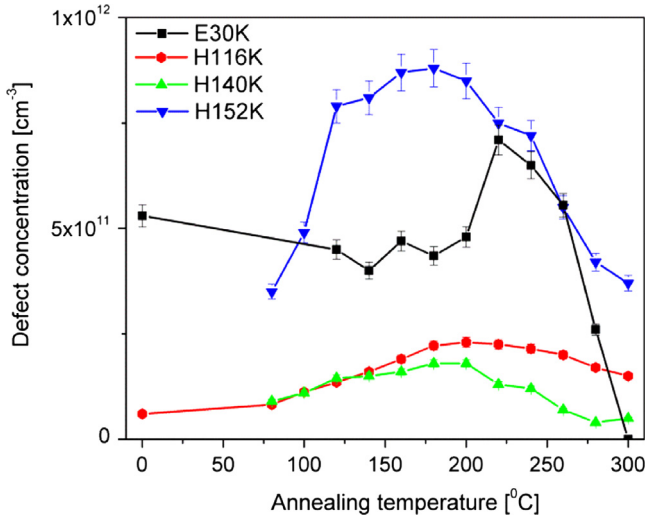
Fig. 3. Development of the defect concentration of E (30 K), H (116 K), H (140 K) and H (152 K) in DOFZ material after irradiation with 6 MeV electrons for a fluence $\Phi = 6 \times 10^{14}$ cm^{-2}. The data were obtained after isochronal annealing for a heat treatment of 30 min at each temperature.

Fig. 4b) shows the development of the effective doping concentration from C–V measurement as function of annealing time at 80 °C. A very pronounced beneficial effect of the oxygen content was observed. While the STFZ samples undergo a space-charge sign inversion, SCSI (change of the space-charge sign from initially positive in n-type silicon to negative, i.e. effectively p-type material) at about 100 min at 80 °C, the oxygenated diodes did not show this up to 30.000 min at 80 °C. These "macroscopic" differences are due to the presence of both, the I$_p$ defect, a deep acceptor-like defect, generated mainly in STFZ (the I$_p$ defect is formed via VO as suggested by theV$_2$O generation model [31,32]) responsible for the SCSI effect, and the lower concentration of the E (30 K) defect, a shallow donor in the upper half of the gap, which

causes the increase of the positive space charge. The H (116 K), H (140 K) and H (152 K) defects are created in both materials with almost the same introduction rate.

Experimental and theoretical evidence for the identification of the electronic structure of basic defects in silicon, such as the vacancy and di-vacancy, are discussed in [33,34]. Recently the structure and electronic properties of the tri-vacancy (V$_3$) have been identified. Using Laplace DLTS and different stress conditions it was found to be a bi-stable center with two configurations (four-fold and planar). In the planar configuration V$_3$ gives rise to two acceptor levels at $E_c-0.36$ eV and $E_c-0.46$ eV which were correlated with the annealing behavior of the reverse current [35,36]. As observed (see Fig. 6a in Section 6) with increasing the electron energy more and more di-vacancies and tri-vacancies are generated suggesting that these defects can be produced directly by irradiation and not by pairing single vacancies. Thus, considering that by increasing the electrons energy, also the recoil energy increases it may become possible to knockout more than one atom from the lattice. Since tri-vacancies become mobile at temperatures higher than 200 °C, it is very likely that they are trapped by impurities. One probable possibility is the trapping of tri-vacancies by oxygen, thus forming the V$_3$O defect.

From TSC measurements after annealing at high temperatures we detected in DOFZ Si two new hole defects, labeled H (87 K) and H (98 K) with energy levels at $E_V+0.193$ eV and $E_V+0.234$ eV, respectively. In Fig. 5a) typical TSC spectra after annealing at different temperatures are shown, where the filling of the traps was performed by illuminating the diode with 520 nm light from the rear side (hole injection).

The comparison between STFZ and DOFZ material presented in Section 5 shows that oxygen plays an important role. Both defects H (87 K) and H (98 K) were detected only in DOFZ. The origin and structure of these two defects are unknown. In [37] the activation energies of these levels are associated with the donor levels of the tri-vacancy (V$_3$) and tri-vacancy-oxygen (V$_3$O) complex. The annealing behavior of H (87 K) showed that the concentration of this defect is constant up to 180 °C then the defect anneals in very
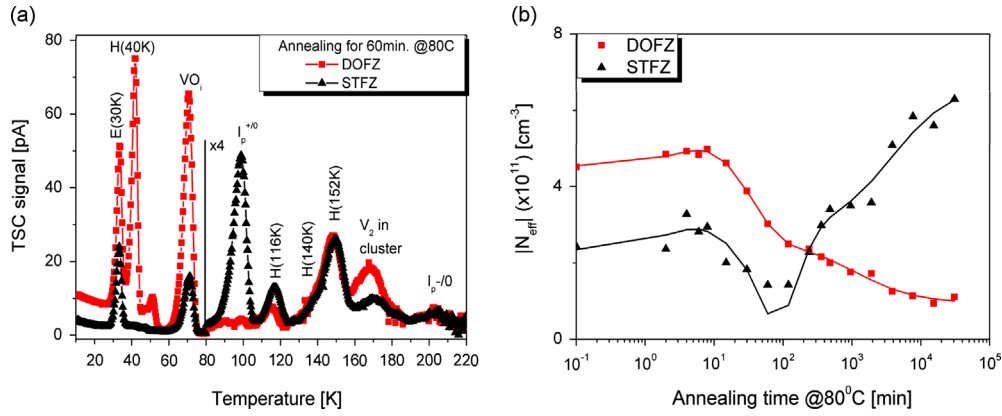
Fig. 4. (a) TSC spectra for irradiation with 6 MeV electrons, $\Phi = 1 \times 10^{15}$ cm^{-2}, after annealing for 60 min at 80 °C. (b) Annealing behavior of the radiation-induced change in the effective doping concentration at 80 °C, from CV measurements, for the same energy and fluence as in (a); solid line represents the dependence described by the Hamburg model [21].
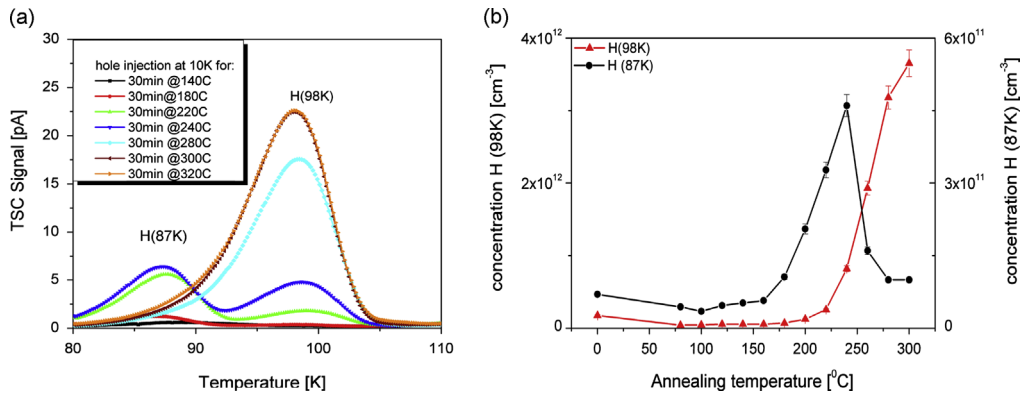

Fig. 5. (a) TSC spectra of a DOFZ diode irradiated with 6 MeV, $\Phi = 6 \times 10^{14}$ cm^{-2}, after isochronal annealing. The filling of the traps is performed by illumination from the rear side (hole injection). (b) Defect concentrations as function of annealing temperature for H (87 K) and H (98 K) evaluated from TSC measurements on electron-irradiated DOFZ material (temperature increment: 20 °C, time at each temperature: 30 min).

quickly, with a maximum concentration at 240 °C. Then it completely anneals out at 300 °C. Therefore an association of this defect with the donor level of the tri-vacancy is questionable. For the H (98 K) defect an increase of its concentration is observed for temperatures higher than 220 °C (Fig. 5b). This annealing behavior and the fact that the H (98 K) defect is a hole trap with the above mentioned activation energy indicate that the H (98 K) defect might be attributed to the overlap of the donor states of V_2O and V_3O [37]. Further studies are ongoing in order to obtain an insight into the mechanism responsible for the annealing behavior of these two defects.

6. DLTS measurements: energy dependence

Fig. 6a shows the recorded DLTS spectra of electron traps obtained from p$^+$–n diodes after irradiation with electrons of different energies. The spectra have been normalized to the amplitude of the $V_2^{=/-}$ signal in order to show a clearer picture of the energy dependence of the introduction of the single-vacancy related defect VO and the tri-vacancy defect complex V_3.

The main damage caused by irradiation with 1.5 MeV electrons is due to introduced point defects, which originate from primary-generated interstitials and vacancies. Single vacancies are mobile at room temperature. Therefore vacancy defects will be distributed uniformly in the bulk. On the other hand, the di-vacancies are created in much lower concentration than single vacancies (the spectra in the range between 100 K and 300 K are magnified by a

factor of 5). For 3.5 MeV electrons the recoil energy is sufficiently high to knock out secondary atoms frequently. This does not lead to more single vacancies, but di-vacancies and tri-vacancies (V_2, V_3) are directly generated. This effect becomes more dominant when irradiating with higher energy electrons. It results in a decrease of the VO introduction rate and an increase of V_2 and V_3. In Fig. 6b the introduction ratios for the double negative charged di-vacancy and tri-vacancy with respect to the single vacancy related VO defect are shown as function of the electron energy. A steady increase with increasing energy is observed for both ratios.

Finally it should be mentioned that the bi-stability of the V_3 defect could be correlated with the bi-stability of the dark current [38]. It was also found that the V_3 defect is responsible for about 60% of the dark current for neutron-irradiated diodes [39]. Therefore, also for the electron-irradiated devices at least part of the dark current should be due to the creation of the tri-vacancies.

7. Summary and conclusions

First results have been presented on systematic studies on radiation damage induced by mono-energetic electrons in the kinetic energy range from 1.5 MeV to 15 MeV. This work aims at a better understanding of the defect-formation mechanisms leading to isolated point defects and cluster defects.

The microscopic damage produced in n-type high-resistivity silicon diodes fabricated of different materials by electrons with
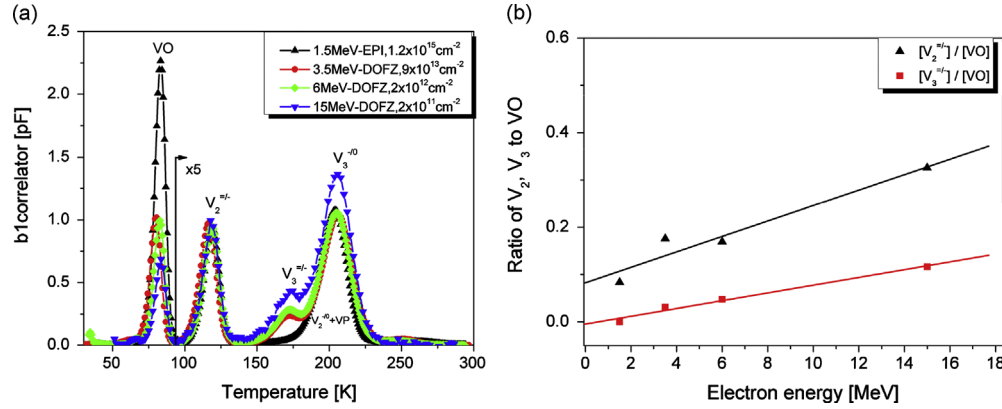
Fig. 6. (a) DLTS spectra of electron traps showing the energy dependence for EPI-ST (electron kinetic energy: 1.5 MeV) and DOFZ (3.5, 6, and 15 MeV) for different fluence values. The spectra are normalized to $V_2^{=/-}$. The DLTS parameters used are: reverse bias $U_R = -10$ V, pulse voltage $U_P = -0.1$ V, fill time $t_{fill} = 100$ ms, and time window $T_W = 200$ ms. (b) Ratio of the concentrations for di-vacancy (V_2), tri-vacancy (V_3) and the single vacancy defect as function of electron energy.

energies between 1.5 and 15 MeV for fluences up to 10^{15} cm^{-2} has been investigated. Measurements of macroscopic properties (I/V and C/V) allowed evaluating the current-related damage parameter α. The energy dependence of α was compared to calculations of the Non-Ionizing-Energy-Loss (NIEL) for electrons. It was found that the α scale better with the "effective" NIEL values especially at low electron energies, compared to the "classical" NIEL. The direct comparison of the introduction rate of defects with the "effective" NIEL is the object of an ongoing analysis of the microscopic data.

The energy levels produced by electron irradiation have been studied by using microscopic defect spectroscopy (DLTS and TSC) in the temperature range from 10 K to 300 K. As expected, it has been found that the ratio between the concentrations of cluster-related defects and of point defects increase with electron energy.

TSC measurements have shown an increase of the concentration of the donor-like defect E(30 K) and of a group of acceptors, with energy levels in the lower half of the band gap, when the electron energy is increased. These defects were also observed for high-energy proton and neutron irradiation, and were attributed to cluster-related defects.

By comparing the results on radiation damage in oxygen-lean with oxygen-enriched material, we conclude that: (i) E (30 K) is an oxygen-related defect, as its introduction rate is almost 3 times larger in DOFZ than in STFZ. (ii) During the first 30.000 min of annealing at 80 °C the STFZ material undergoes type inversion while the DOFZ diodes do not show it. This is mainly due to the presence of the I_p defect and a much smaller concentration of E (30 K) in STFZ diodes. (iii) After isochronal annealing the concentration of E (30 K) defect and of the H defects (H (116 K), H (140 K) and H (152 K)) were determined. It has been observed that all these defects start to anneal out nearly at the same temperature of 200 °C. (iv) In DOFZ we were able to identify the donor level of the V_3O defect, by performing TSC measurements with hole injection by light of 520 nm.

From DLTS measurements ratio of di-vacancies and tri-vacancies concentration to that of single vacancies was evaluated. It was shown that both ratios increase with increasing energy. At electron energy of 1.5 MeV only point defects are created, whereas with increasing electron energy di-vacancies and tri-vacancies are directly created.

With the help of isothermal-annealing studies, the relation between specific defects and macroscopic parameters, like dark current and effective doping, and the defect kinetics could be established. However, further studies are needed. The understanding of the defect formation and further studies of the impact of defects on detector performance are important for improving the radiation hardness of silicon sensors by defect engineering.

References

[1] O. Bruning, et al., Journal of Physics Conference Series 110 (2008) 112002.
[2] J. Metcalfe, Nuclear Physics B (Proceedings Supplements) 215 (2011) 151–153.
[3] RD50, ⟨http://www.cern.ch/rd50⟩.
[4] I. Pintilie, L. Pintilie, M. Moll, E. Fretwurst, G. Lindstroem, Applied Physics Letters 78 (2001) 550.
[5] J. Stahl, E. Fretwurst, G. Lindstroem, I. Pintilie, Physica B 340 (2003) 705.
[6] M. Scaringella, D. Menichelli, M. Bruzzi, et al., Nuclear Instruments and Methods in Physics Research Section B 570 (2007) 322–329.
[7] G. Lindstroem, et al., Nuclear Instruments and Methods in Physics Research Section A 568 (2006) 66–71.
[8] E. Fretwurst, et al., Nuclear Instruments and Methods in Physics Research Section A 583 (2007) 58–63.
[9] I. Pintilie, et al., Nuclear Instruments and Methods in Physics Research Section A 556 (2006) 197–208.
[10] I. Pintilie, E. Fretwurst, G. Lindstroem, Applied Physics Letters 92 (2008) 024101.
[11] I. Pintilie, et al., Nuclear Instruments and Methods in Physics Research Section A 611 (2009) 52–68.
[12] A. Junkes, et al., Physica B 407 (2012) 3013–3015.
[13] CiS, ⟨http://www.cismst.org⟩.
[14] IPEN-CNEN/SP, ⟨https://www.ipen.br⟩.
[15] BUS, ⟨http://www.bsu.by⟩.
[16] PTB, ⟨http://www.ptb.de⟩.
[17] ELBE, ⟨http://www.hzdr.de⟩.
[18] D.V. Lang, Journal of Applied Physics 45 (1974) 3023.
[19] L. Forbes, C.T. Sah, Solid-State Electron 14 (1971) 182.
[20] S. Weiss, R. Kassing, Solid-State Electron 31 (12) (1988) 1733.
[21] M. Moll, Ph.D. thesis, University of Hamburg, DESY-THESIS-1999-040, December 1999.
[22] I. Pintilie, et al., Nuclear Instruments and Methods in Physics Research Section A 476 (2002) 652–657.
[23] RD48, ⟨http://rd48.web.cern.ch/rd48⟩.

[24] G. Lindstroem, Nuclear Instruments and Methods in Physics Research Section A 512 (2003) 30–43.
[25] G.P. Summers, et al., IEEE Transactions on Nuclear Science NS40 (6) (1993) 1379.
[26] C. Inguimbert, et al., IEEE Transactions on Nuclear Science NS57 (2010) 41915.
[27] A. Akkerman, et al., Radiation Physics and Chemistry 62 (2001) 301–310.
[28] P. Arnolda, et al., IEEE Transactions on Nuclear Science NS58 (2011) 3.
[29] G. Lindstroem, Nuclear Instruments and Methods in Physics Research Section A 512 (2003) 30–43.
[30] I. Pintilie, et al., Applied Physics Letters 81 (2002) 165.
[31] I. Pintilie, et al., Nuclear Instruments and Methods in Physics Research Section A 14 (2003) 18.
[32] I. Pintilie, et al., Applied Physics Letters 82 (13) (2003) 2169–2171.
[33] G.D. Watkins, J.W. Corbett, Physical Review 138 (1965) A543.
[34] V.P. Markevich, et al., Journal of Physics Condensed Matter 15 (2003) S2779.
[35] V.P. Markevich, et al., Physical Review B80 (2009) 235207.
[36] V.P. Markevich, et al., Physica B 404 (2009) 4565–4567.
[37] V.P. Markevich, et al., Physica Status Solidi A 208 (2011) 568–571.
[38] R.M. Fleming, et al., Journal of Applied Physics 111 (2012) 023715.
[39] A. Junkes, et al., Nuclear Instruments and Methods in Physics Research Section A 612 (2010) 525–529.
[40] G.D. Watkins, Materials Science in Semiconductor Processing 3 (2000) 227–235.
[41] L.W. Song, et al., Physical Review Letters 60 (1988) 460–463.
[42] L.W. Song, et al., Physical Review B 42 (1990) 5765.